Single-shot spatially modulated Stokes polarimeter based on a GRIN lens

Jintao Chang,[1,2] Nan Zeng,[2] Honghui He,[2] Yonghong He,[2] and Hui Ma[1,2,*]

[1]*Department of Physics, Tsinghua University, Beijing 100084, China*

[2]*Shenzhen Key Laboratory for Minimal Invasive Medical Technologies, Graduate School at Shenzhen, Tsinghua University, Shenzhen 518055, China*

**Corresponding author: mahui@tsinghua.edu.cn*

Received January 22, 2014; revised February 25, 2014; accepted March 26, 2014; posted March 27, 2014 (Doc. ID 205217); published April 23, 2014

A new polarimeter for the simultaneous measurement of all Stokes parameters in a single shot is presented. It consists of only a gradient index (GRIN) lens, a polarizer, an imaging lens, and a CCD, without mechanical movements, electrical signal modulation, or the division of amplitude components. This design takes advantage of the continuous spatial distributions of birefringence value and the fast axis direction of a GRIN lens and derives the state of polarization (SOP) of the incident beam from the characteristic patterns on the CCD images. Tests show that this polarimeter is very accurate even with low-resolution images. It is versatile and adapts to light sources of different wavelengths. It is also very stable, robust, low cost, and simple to use.

OCIS codes: (120.5410) Polarimetry; (110.2760) Gradient-index lenses; (130.5440) Polarization-selective devices; (120.2130) Ellipsometry and polarimetry.

http://dx.doi.org/10.1364/OL.39.002656

Polarimeters are used to characterize the state of polarization (SOP) of light and are widely applied in areas ranging from optical biopsy [1] and material characterization [2] to remote sensing of the Earth and astronomical bodies [3]. Many polarimeters adopt temporal polarization modulation and time sequential data acquisition using rotating elements [4], photoelastic modulators [5], or liquid crystal retarders (LCR) [6]. These polarimetries have been extensively studied and many optimization techniques have been developed [3–8]. However, such time sequential techniques are likely to be subject to artifacts due to instabilities in the sample or the optical system during data acquisition.

There are also many techniques for simultaneous measurement polarimeters (SMP) [7] that divide the input beam into different subbeams and project them simultaneously to different polarization analyzers in a spatial domain or a spectral domain. Simultaneous detections of Stokes parameters are achieved using multiple detectors [9–11], spatial modulation [12–14], or spectral modulation [15]. Recently, there have been consistent efforts to make spatially modulated devices, such as the handmade axisymmetrical quarter wave plates [12], thin film micropolarization array deposited on the CMOS imaging sensor [13], and the radial polarizer fabricated by atomic force microscope stroking method [16], all of which require sophisticated fabrication techniques to maintain high precision and reproducibility.

In this Letter, we propose a new spatially modulated polarimeter based on a gradient index (GRIN) lens that measures the Stokes parameters simultaneously and takes full advantage of the optimization techniques in rotating elements and LCR polarimeters.

The GRIN lenses are commonly used as objectives and rod lenses for small diameter imaging systems, where conventional lenses are not suitable due to size limitation. Instead of a fixed refractive index and curved surfaces in a conventional lens, a radial GRIN lens has a gradient refractive index profile and flat surfaces. During the fabrication, the ion-exchange process introduces stresses along the radial direction of the GRIN lens rod and induces an intrinsic birefringence [17,18]. Such birefringence has to be minimized as a source of aberration for normal applications, but is explored in this Letter for spatial polarization modulation. Along the azimuth, it is similar to a rotating wave plate device keeping the birefringence value fixed but rotating the fast axis direction over a full circle. Along a radial axis, a GRIN lens is similar to a LCR device in the temporal domain varying continuously its birefringence value at a fixed fast axis direction. Many existing knowledge and techniques on temporal modulation polarimetry can be applied to the GRIN lens polarimetry for achieving better accuracy and stability.

The schematic of the experimental setup is shown in Fig. 1. Incident beams of different SOPs are generated with the PSG consisting of a collimated LED source, a band pass filter (Thorlabs, CWL = 632.8 nm, FWHM = 3 nm), a linear polarizer (Thorlabs, extinction ratio > 5000 : 1), and a quarter wave plate (Thorlabs, 633 nm, retardance accuracy: $\lambda/300$) mounted on a high-precision motorized rotation stage (Thorlabs, PRM1Z8E). The

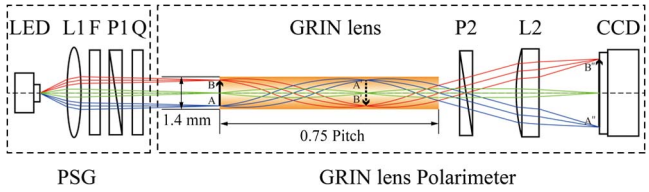

Fig. 1. Optical layout of the polarization state generaator (PSG) and the GRIN lens polarimeter. The diameter of the GRIN lens is 1.4 mm and the pitch is 3/4. L1, collimating len;, L2, imaging lens; F, band pass filter; P1 and P2, polarizer; and Q, quarter wave plate. The CCD is placed at the imaging plane ($A''B''$) of the front surface of the GRIN lens (AB). In this Letter the incident rays are nearly parallel. Birefringence value increases along the radial direction, and the larger birefringence value is displayed with a darker orange color; thus, the red and the blue rays would experience larger linear retardance than the green rays.

optical layout of the GRIN lens polarimeter is very simple. It consists of only a GRIN lens, a polarizer, an imaging lens, and a CCD. It does not need mechanical movements, electrical signal modulation, or beam splitting. The GRIN lens is a spatially modulated device that acts as an assembly of tiny wave plates with different birefringence values and fast axis directions. After passing through the GRIN lens and the angle-fixed polarizer, incident beams with different SOPs generate different characteristic patterns on the CCD. In principle, we can choose only four pixels in the pattern to calculate the SOP of the incident beam. However, we can also take advantage of a much larger number of pixels to reduce the variance of the measurements. Polarimeters based on such a new design are very accurate, simple, stable, robust and low cost.

In this Letter, we use a GRIN lens 60 mm long, 1.4 mm in diameter, and 0.1 NA, supplied by FEMTO TECHNOLOGY CO. LTD. Its polarization property is fully characterized by taking the transmission Mueller matrix and the Lu–Chipman decomposition [19]. The polarization property of the GRIN lens is dominated by its linear retardance. Contributions due to diattenuation and depolarization are much smaller. The profile of the linear retardance is radial, as shown in Figs. 2(a) and 2(c), and the profile of the fast axis direction is azimuthal, as shown in Figs. 2(b) and 2(d). When a paraxial beam of homogeneous SOP enters the front surface of the GRIN lens, it can be regarded as n identical sub-beams incident to n tiny wave plates of different retardances and fast axis directions. Due to the centrosymmetric distribution of the birefringence, there are $n/2$ totally different wave plates. Incident sub-beams of the same SOP emerge with different SOPs after the GRIN lens. After passing through a fixed polarizer, these sub-beams form characteristic intensity patterns at the image plane of the front surface of the GRIN lens. The images are recorded by a CCD (Qimaging Retiga Exi, 12 bit, 1392×1040 pixels). In this Letter, only a small fraction of the CCD images (280×280 pixels) are used for data reductions.

According to typical Mueller matrix expressions of a wave plate and a polarizer, we can derive the expression for the intensity pattern from the CCD corresponding to different incident SOPs. If the Stokes vector of the incident beam to be measured is denoted by S, and the Mueller matrices of the polarizer and the GRIN lens are denoted by M_P and M_{GRIN}, the Stokes vector of the exiting beam S' is given by

$$S' = M_P \cdot M_{\mathrm{GRIN}} \cdot S, \tag{1}$$

where $S = (s_0, s_1, s_2, s_3)^T$ and $S' = (s'_0, s'_1, s'_2, s'_3)^T$. The superscript T represents the transpose operator.

In the calculations, we use only the first row of the Mueller matrix elements of a linear polarizer because a CCD measures only the light intensity. The first row of the Mueller matrix of a linear polarizer is

$$M_P(1,:) = (p_t + p_e, (p_t - p_e)\cos 2\theta_P, (p_t - p_e)\sin 2\theta_P, 0), \tag{2}$$

where p_t and $p_e (p_t > p_e)$ are the transmission ratios in the transmission axis and extinction axis, and θ_p is the orientation of the transmission axis. The extinction ratio p_t/p_e of a common linear polarizer is beyond 5000; thus, p_e can be ignored when measuring s'_0. On the other hand, θ_p must be fixed carefully to the target angle, because a small angle offset can generate a significant difference. In our experiments, the polarizer is fixed with its transmission axis along the horizontal orientation, but the following discussions can also be extended to any other fixed orientations. Ignoring p_e, Eq. (2) reduces to

$$M_P(1,:) = (p_t, \quad p_t, \quad 0, \quad 0). \tag{3}$$

If we ignore the small diattenuation and depolarization of the GRIN lens, its Mueller matrix M_{GRIN} can be regarded as a set of Mueller matrix $M_{\mathrm{GRIN}n}$ for the n tiny wave plates. $M_{\mathrm{GRIN}n}$ is given as:

$$M_{\mathrm{GRIN}n} \approx \begin{pmatrix} 1, & 0, & 0, & 0 \\ 0, & \cos^2 2\theta_n + \sin^2 2\theta_n \cos\delta_n, & 0.5 \sin 4\theta_n (1 - \cos\delta_n), & -\sin 2\theta_n \sin\delta_n \\ 0, & 0.5 \sin 4\theta_n (1 - \cos\delta_n), & \sin^2 2\theta_n + \cos^2 2\theta_n \cos\delta_n, & \cos 2\theta_n \sin\delta_n \\ 0, & \sin 2\theta_n \sin\delta_n, & -\cos 2\theta_n \sin\delta_n, & \cos\delta_n \end{pmatrix}, \tag{4}$$

where δ_n and θ_n are the retardance and fast axis direction of the nth wave plate, respectively.

In a real experiment, the subscript n corresponds to the number of pixels in the CCD image of the GRIN lens. Different values for n represent different pixels, or the different tiny wave plates. All the n measurements are carried out simultaneously, or in a single shot.

Substituting Eqs. (3) and (4) into Eq. (1), we have

$$\begin{aligned} s'_{0n} = {} & p_t s_0 + p_t(\cos^2 2\theta_n + \sin^2 2\theta_n \cos\delta_n) s_1 \\ & + 0.5 p_t \sin 4\theta_n (1 - \cos\delta_n) s_2 - p_t \sin 2\theta_n \sin\delta_n s_3. \end{aligned} \tag{5}$$

The intensity on the nth pixel is proportional to s'_{0n}, and the intensities of all pixels on the CCD can be expressed in a matrix form:

$$I = A \cdot S, \tag{6}$$

where the intensity is expressed as

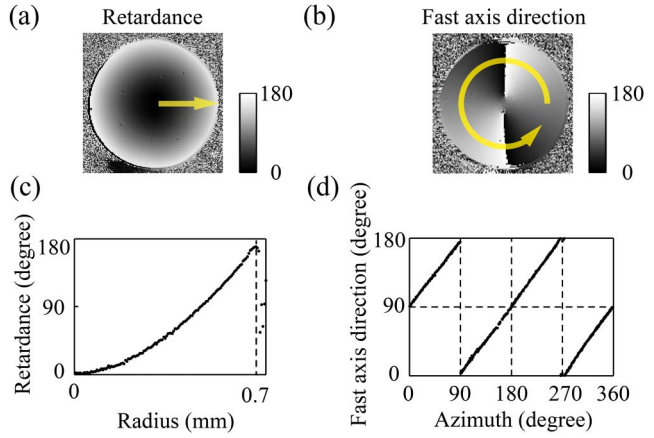

Fig. 2. Spatial distributions of linear retardance (a) and (c) and fast axis direction (b) and (d) of a GRIN lens 60 mm long, 1.4 mm in diameter, and 0.1 NA.

$$I = (s'_{01}, \quad s'_{02}, \quad s'_{03}, \quad \cdots, \quad s'_{0n})^T. \tag{7}$$

Here, A is a $n \times 4$ ($n \geq 4$) rectangular data reduction matrix determined from the experimental data. When $n > 4$, there are more equations than unknowns and S is overdetermined. The least-squares estimate for S utilizes a particular matrix inverse, the pseudoinverse A_p^{-1} of A [3]. Finally, I and A determine S,

$$S = A_p^{-1} \cdot I. \tag{8}$$

In the following part of this Letter, we use the premeasured Mueller matrix of the GRIN lens M'_{GRIN} instead of M_{GRIN} to determine A. M'_{GRIN} takes into account not only the linear retardance (M_{GRIN}), but also the diattenuation and the depolarization, which are usually very small but could affect the accuracy of measurements.

Incident beams of different SOPs are encoded into patterns of different shapes on the CCD. Figure 3(a) shows the typical patterns corresponding to some common SOPs, and the patterns will gradually disappear when the degrees of polarization (DOP) of the incident beams decrease.

For each pattern on the CCD, we can use at least four pixels or all the pixels to derive the incident SOP. Experiments with different selections of the pixels result in different accuracies. It is necessary to locate regions on the image that produce the optimal data reduction matrix A. We can choose only four pixels of the same retardance but different fast axis directions, corresponding to the four minimum measurements in a rotating wave plate system [4,8]. However, in order to reduce the variance of the measurements, we can also choose more pixels using the rotating wave plate scheme, in which data are taken at angles spaced uniformly over 360° and Stokes parameters are derived by a discrete Fourier transform [4,8]. To achieve this, we divide the image into concentric annular subregions with different retardances, shown in Fig. 3(b). Each annular subregion, indicated by subscript i, contains n_i pixels corresponding to n_i measurements taken with a wave plate of fixed retadance but rotated uniformly over 360°. For

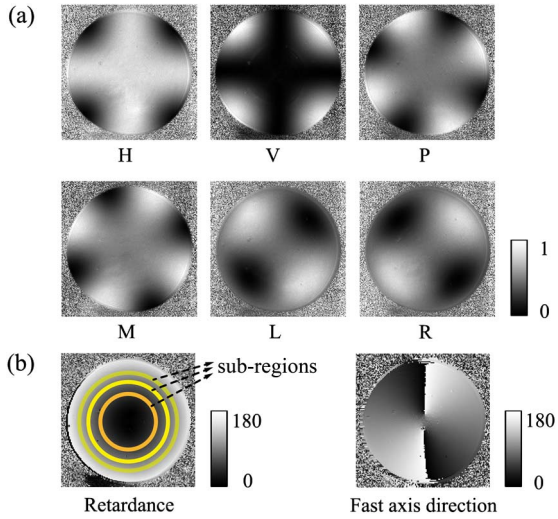

Fig. 3. (a) Experimental images from the CCD corresponding to linearly polarized incident lights at 0° (H), 90° (V), 45° (P), and 135° (M), and the left (L) and right (R) hand circularly polarized lights. Note Fig. 3(a) $H \sim R$ are normalized pixel by pixel with the image for the unpolarized beam. (b) Retardance and fast axis profiles of the GRIN lens, some subregions with different retardance are plotted with different colors. The size of the images of (a) and (b) is 280×280 pixels.

the GRIN lens we used, the linear retardances in different subregion δ_i, vary from 0° at the center to nearly 180° at the edge.

We use condition number (CN) to quantify if the matrix A is well-conditioned [3] and equally weighted variance (EWV) to assess the noise immunity of the polarimeter [4]. To evaluate the actual performance, or the SOP accuracy of the polarimeter [20], we calculate the angular accuracy (the intersection angle between the measured and calculated Stokes vectors on the Poincare Sphere) and the DOP accuracy.

For each incident beam, we divide the image into annular subregions of equal retardances that are then used to derive the SOP. To minimize both the EWV of A and the variance of the measurements, we expand each annular subregion at 10° retardance intervals to include more pixels in the calculations of I and A. In the PSG, we keep the polarizer fixed and rotate the wave plate in 3° equal steps over 180° to generate 60 different SOPs. For all the annular subregions, the CNs and the mean angular accuracies of the 60 measurements are calculated and plotted over the 15°–160° range, as shown in Fig. 4. It should be noted that the area of a subregion depends on its radius and width. It does not change linearly with the radius due to the radial retardance profile of the GRIN lens (Fig. 2c). In Fig. 4, each subregion has more than 3000 pixels. In the subregions ranging from 0° to 15° and 160° to 180°, n_i diminishes sharply. Fig. 4 shows that CN is a good indicator to describe how sensitively the system responds to errors in the measurements. The angular subregion accuracies distribution follows the trend of the CN. In the low CN regions, the value and the variance of the angular accuracies are much smaller than in the higher CN regions (Fig. 4). The DOP accuracy distribution is similar with that of the angular accuracy.

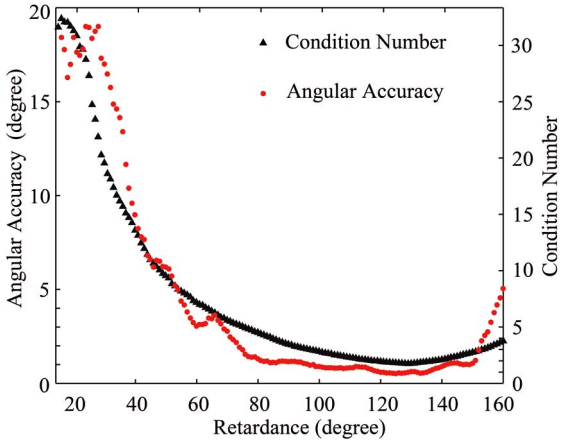

Fig. 4. CNs of the 146 annular subregions ranging from 15° to 160°, and the mean angular accuracies of the 60 measurements for the 146 annular subregions.

The CN in the subregions around 130° is very close to the optimal value 1.732 [8,11], and the angular accuracy can reach to 0.6°. The mean angular accuracy between 80° and 150° retardance is 0.96°. As an example, Fig. 5 shows the Stokes parameters s_1, s_2 and s_3 derived from the pixel data in the 130° retardance subregion. The deviations between the experimental and the calculated Stokes parameters are very small.

The above experimental results prove that we are able to measure the SOP of an incident beam very accurately using a GRIN lens as a spatial modulation device in a single shot as far as the proper region on the CCD is selected. Although only a small fraction of the CCD (280×280 pixels) is used in the tests, the redundant data still allow satisfactory measurement accuracy. Preliminary tests also show that the measurement accuracy can be maintained even with a smaller image size, allowing the possibility of using a consumer grade low-resolution and low-cost 2D detector for such polarimeters.

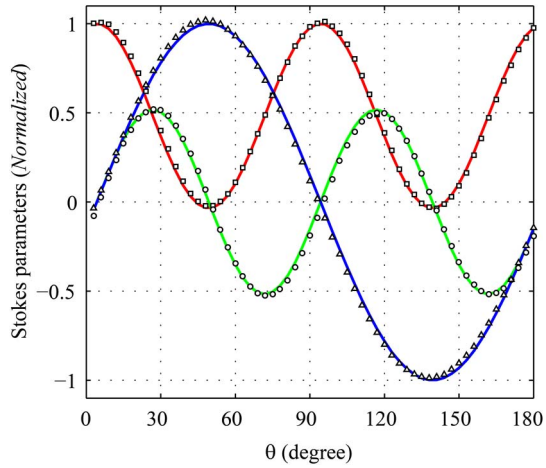

Fig. 5. Experimental (square marker, s_1; circle marker, s_2; triangle marker, s_3) and calculated (red line, s_1; green line, s_2; blue line, s_3) Stokes parameters corresponding to different incident SOPs, where in the PSG the polarizer is fixed and the wave plate is rotated 180° in 60 equal steps. The patterns on the CCD are recorded (see Media 1).

There are a number of distinctive advantages for this polarimeter design. The system determines all the Stokes parameters accurately and simultaneously. Even with a low-resolution 2D detector, the large amount of pixels still provide redundant data to reduce the variance of the measurements. It is very simple, consisting of only a GRIN lens, a polarizer, a normal imaging lens, and a 2D detector. With proper design of the GRIN lens, even the imaging lens is optional, and the polarizer can be reduced to a thin film coated on the rear surface of the GRIN lens. The system does not need any mechanical moving parts or electrical modulators; therefore is easy to miniaturize. It is very stable, robust, low cost, and easy to use. It is also versatile and adapts to light sources of different wavelengths. A limitation of this polarimeter is that it is not an imaging polarimeter. The incident beam should have uniform SOP across the front surface of the GRIN lens. The small collection angle (0.1 NA in this work) can be another limitation of this polarimeter.

This new polarimeter will make the SOP measurement easier and cheaper, and promote new applications of polarimetry. It should also stimulate further studies on GRIN lenses as polarization optics.

We acknowledge financial support from the National Natural Science Foundation of China (NSFC) Grant Nos. 11174178, 61205199, and 11374179. We also thank Mr. Z. Liu from Femto Technology Co. Ltd. for the discussions on GRIN lenses.

References

1. M. R. Antonelli, A. Pierangelo, T. Novikova, P. Validire, A. Benali, B. Gayet, and A. D. Martino, Opt. Express **18**, 10200 (2010).
2. R. M. A. Azzam and N. M. Bashara, *Ellipsometry and Polarized Light* (North-Holland, 1987).
3. R. A. Chipman, *Handbook of Optics*, 3rd ed. (McGraw-Hill, 2009, Vol. **1**.
4. D. S. Sabatke, M. R. Descour, E. L. Dereniak, W. C. Sweatt, S. A. Kemme, and G. S. Phipps, Opt. Lett. **25**, 802 (2000).
5. S. Alali, T. Yang, and I. A. Vitkin, Opt. Lett. **38**, 2997 (2013).
6. A. D. Martino, Y. K. Kim, E. G. Gaurel, B. Laude, and B. Drevillon, Opt. Lett. **28**, 616 (2003).
7. C. F. LaCasse, R. A. Chipman, and J. S. Tyo, Opt. Express **19**, 14976 (2011).
8. J. S. Tyo, Appl. Opt. **41**, 619 (2002).
9. R. M. A. Azzam, Opt. Acta **29**, 685 (1982).
10. R. M. A. Azzam, Opt. Lett. **10**, 309 (1985).
11. A. Peinado, A. Turpin, A. Lizana, E. Fernandez, J. Mompart, and J. Campos, Opt. Lett. **38**, 4100 (2013).
12. T. Wakayama, Y. Otani, and T. Yoshizawa, Proc. SPIE **7461**, 74610M (2009).
13. V. Gruev, A. Ortu, N. Lazarus, J. V. Spiegel, and N. Engheta, Opt. Express **15**, 4994 (2007).
14. J. S. Tyo, C. F. LaCasse, and B. M. Ratliff, Opt. Lett. **34**, 3187 (2009).
15. F. Snik, T. Karalidi, and C. U. Keller, Appl. Opt. **48**, 1337 (2009).
16. I. Nishiyama, N. Yoshida, Y. Otani, and N. Umeda, Meas. Sci. Technol. **18**, 1673 (2007).
17. W. Su and J. A. Gilbert, Appl. Opt. **35**, 4772 (1996).
18. J. L. Rouke and D. T. Moore, Appl. Opt. **38**, 6574 (1999).
19. S. Y. Lu and R. A. Chipman, J. Opt. Soc. Am. A **13**, 1106 (1996).
20. X. S. Yao, X. Chen, and L. Yan, Opt. Lett. **31**, 1948 (2006).